Influence of Electroslag Weld Metal Composition on Hydrogen Cracking

The number of hydrogen cracks and their average length in welds are related to weld metal composition and microstructure

BY R. THIBAU AND S. R. BALA

ABSTRACT. The presence of hydrogen in electroslag weld metal is known to produce effects such as the micro-cracking in the weld metal along proeutectoid ferrite veins. The present work investigated the relationship of the atmospheric humidity, the diffusible hydrogen, the alloying elements, the microstructure, and the cracking behavior of the weld metal. The weld metal was obtained by butt-joining A36 plates using a consumable guide electroslag-single electrode process with Arcos BV flux. The composition of the weld metal was varied in the low alloy content ranges by welding with one of seven commercially available electrodes.

The humidity above the weld was monitored and kept constant at two different levels representative of an extremely humid, and a normal ambient atmosphere.

Usually higher hydrogen contents were found at the bottom of the welds (2–12 $cm^3/100g$) compared to the rest of the weld (1.7–4.4 $cm^3/100g$). An increase of 50% of moisture content in the atmospheric humidity yielded a 40% increase in the average diffusible hydrogen (from 2.8 to 3.9 $cm^3/100g$).

The number of cracks, their total length and average length for each weld were measured. These were related to the weld metal hydrogen content and chemical composition, using a multilinear regression analysis. Due to the 40% increase in diffusible hydrogen content, the average number of cracks per weld was increased by a factor of $\sim$ 3.5 while the average crack length was increased by a factor of 1.4 (from 3.9 to 5.5 mm or 0.15 to 0.22 in.).

As expected, electrodes containing higher Cr, Mo, Mn, C or Ni contents yielded a refined microstructure with smaller proeutectoid ferrite grains as compared to the ones obtained with the rest of the wires. Microstructures showing no proeutectoid ferrite veins cracked along the prior austenite grain boundary.

Carbon and H_2 enhanced both the nucleation and the propagation stages of cracking. Sulfur in the form of manganese sulfide inclusions played the role of a hydrogen sink and, therefore, increased the number of cracks but decreased their average length. Titanium at very low contents decreased the number of cracks and at the same time increased their average length. Elements such as Cr and Ni up to a maximum of 0.5 and 2%, respectively, were found to reduce the length of hydrogen cracks whereas Si and Cr acting as ferrite hardeners were clearly detrimental as far as crack length was concerned. Molybdenum and manganese showed mild effects on the propagation stage and should be considered, in order to achieve mechanical property requirements, only after maximum levels of Cr and Ni are reached.

Introduction

Internal microcracks are known to be present in electroslag weld metals. Hydrogen is generally identified as the cause of such defects. The solubility and diffusivity of hydrogen are important factors regulating the formation of cracks. Many investigators agree that hydrogen is the catalyst for the nucleation and propagation of microcracks.

The phenomenon of hydrogen cracking is known in steel making as well as in the arc welding technologies and has led to appropriate practices such as reducing the plate carbon content as well as the use of low hydrogen electrodes, respectively.

R. THIBAU, formerly with AMCA International, is now a Research Associate with the Industrial Materials Research Institute, N. R. C. Canada, Montreal; and S. R. BALA is with the Research and Technology Centre, AMCA International Limited, Kanata, Ontario, Canada.

Solubility of Hydrogen in Steels

The solubility of hydrogen in iron increases with temperature. However, the solubility of hydrogen in iron also decreases sharply when molten iron solidifies to delta ferrite and when austenite transforms into ferrite. As a consequence, austenite transformation inhibitors such as Ni, Mn, Mo, Cr, C and Ti, with their ability to lower the Ar_3 temperature, should have a tendency to maintain hydrogen in the weld metal for a longer period of time. For the same reason, an increase in the cooling rate may cause an increase in the weld metal hydrogen content.

Diffusivity of Hydrogen in Steels

It is well known that ferrite, besides having a lower solubility for hydrogen, shows a higher diffusivity compared to austenite. However, the diffusivity of hydrogen in ferrite significantly decreases at about 150°C (302°F) (Ref. 1). Also, hydrogen diffusivity should not be influenced significantly by the alloying elements (in solid solution), at least for the levels normally found in low alloy steels (Ref. 2).

Alloying elements control the hydrogen diffusivity by affecting the microstructure of the steel. For example, some data (Ref. 3) indicate that diffusivity is lower in martensite and fine bainite than in pearlite. Also, increasing the pearlite lamellar spacing would decrease the diffusivity (D). The value (Ref. 4) of D generally decreases with the alloying elements except for chromium, which shows a maximum at 0.5-0.8%. The diffusivity of hydrogen is also related to crystal imperfections or microstructural defects such as dislocations, grain boundaries, micro-voids, etc.

Besides its diffusible state, hydrogen can also be found as residual hydrogen, i.e., hydrogen gas or methane in microvoids (Ref. 5) at temperatures above 200°C (392°F). Atomic hydrogen can

segregate at trap sites such as interfaces at coherent and incoherent carbides, inclusions, grain boundaries and dislocation cores (Ref. 6). It was shown (Ref. 7) that coherent titanium carbides form reversible traps and can be beneficial because they uniformly distribute hydrogen. Incoherent TiC form irreversible traps and increase the resistance to cracking as long as they do not accumulate enough hydrogen to nucleate a crack.

Formation of Hydrogen Cracks and Their Fractography

When electroslag weld metal cools, a triaxial state of stress will develop around the longitudinal central axis of the weld. The combination of a stress concentrator with hydrogen may nucleate a crack. The cracking behavior is described by two stages (i.e., nucleation and propagation), which can be quantified by the number of cracks and their average length, respectively, in a given area of the weld metal (Ref. 4, 8). Various theories have been developed to explain this phenomenon in detail, viz., the cohesive energy concept (Ref. 9), the surface energy criteria (Ref. 10), the pressure mechanism (Ref. 11, 12), and the dislocation mechanisms (Ref. 6).

The main practical consequence of hydrogen in steel found by many investigators (Ref. 13-17) are the decreases in ductility or fracture strain; these are comparable to a decrease in temperature or an increase in strain rate. The cracks found in the electroslag weld metal are generally located along the prior austenite grain boundaries (Ref. 18, 19). They usually nucleate and propagate at temperatures lower than 300°C (572°F). The susceptibility to temper embrittlement by P, Sn, and Sb enhanced by elements such as Mn and Si (Ref. 6, 20, 21) may contribute in the crack propagation along the prior austenite grain boundaries. The fractographic features observed in a scanning electron microscope (SEM) can be either intergranular, quasicleavage or even microvoid coalescence if large plastic deformation is allowed to take place.

The crack propagation mode changes from intergranular to transgranular, with respect to the prior austenite grain, when the stress intensity factor K_1 (Ref. 12, 22-24) is increased.

Scope of the Present Work

Much attention has been given to the problems of hydrogen cracking in electroslag welds. Recent studies have revealed the sources and the significance of hydrogen in electroslag welds (Ref. 25). However, information on a systematic study relating the weld metal composition to the hydrogen cracking susceptibility of electroslag welds, performed under industrial atmospheric conditions, is scarce. Such a study was, therefore, undertaken to relate the cracking susceptibility to hydrogen content, composition and microstructure of the electroslag weld metal. Finally, the results obtained were used to formulate guide lines to control the deleterious effect of hydrogen cracks in electroslag weld metals.

Experimental Procedure

Materials Used

The base metal was 63.5 mm (2.5 in.) ASTM Gr A36 steel. Seven commercially available 3.2 mm (⅛ in.) diameter electrodes were used. These were Linde nos. 36, 40, 40B, 44, and 100; Armco W.19; and Lincoln 50—identified, respectively, throughout this paper as L36, L40, L40B, L44, L100, AW19, and Lo50; a 2.4 mm (3/32 in.) diameter Linde 40 electrode was also used. Of the seven, only Linde 36 is shown in the American Welding Society's *Filler Metal Comparison Charts* (AWS A5.0-80) as meeting an AWS classification for electroslag welding consumables, i.e., in this case, AWS EH14-EW.

The low carbon consumable guide had an OD of 13 mm (0.5 in.) and an ID of 4 mm (0.16 in.). Arcos BV flux was used during welding; this had a basicity index (B.I.)* of 3, and its composition was as follows: SiO_2—7.6%; Al_2O_3—26.4%; MnO—0%; CaO— 46.0%; MgO—0%; CaF_2—21.0%.

Atmospheric Moisture Content

Humidified air was blown over the surface of the slag during the whole course of the welding. Two different levels of moisture content were used: a low humidity setup (Ref. 25) that yielded 0.0011 g/s of water (vapor) and a high humidity setup yielding 0.0021 g/s. The ambient atmospheric relative humidity varied from 13% at 20°C (68°F) to 30% at 23°C (73°F).

The object of using two different moisture levels was to obtain two hydrogen levels in the weld metals.

Welding Conditions

The welding procedure used in this program was similar to that described in a previous paper (Ref. 25):

1. The power source used was a constant voltage DC machine producing 600 A at 37 V with the electrode being kept at the positive polarity. The average heat input was 112 kJ · mm^{-1} (2850 kJ · $in.^{-1}$) to perform the consumable guide electroslag welded butt joints.

2. The BV flux was kept in an oven at 200°C (392°F) for at least 24 hours (h) before welding and removed only just prior to the start of the welding.

3. Two 63.5 (thickness) × 760 × 300 mm (2.5 × 30 × 12 in.) A36 plates were prepared for butt joint welding (single electrode) in the longitudinal direction. Four spacers and a starting block were tack welded to the plates to give a constant weld gap width of 25.4 mm (1.0 in). The starting block along with the cooling shoes acted as a sump at the bottom of the weld cavity.

4. The water-cooled copper shoes, 152 mm (6 in.) long, were located on each side of the weld gap. They could be moved manually as the welding progressed and acted as the container wall for the weld metal as well as molten slag. The slag cap height was kept constant at 45 mm (1.75 in.) during the course of electroslag welding by adding 5 g of dry BV flux for every 50 mm (2 in.) of the weld length. The humidified air with known moisture content was continuously blown on to the surface of the molten slag.

5. The electrode feed rates were 38 mm/s (91 ipm) and 55 mm/s (130 ipm) for 3.2 and 2.4 mm (0.126 and 0.094 in.) diameter electrodes, respectively. The average welding time was 45 minutes (min) for the 3.2 mm (0.126 in.) diameter electrodes, corresponding to an average welding speed of 0.2 mm/s (0.5 ipm). For the 2.4 mm (0.094 in.) diameter electrodes, the welding speed was 0.18 mm/s (0.43 ipm).

Measurement of Weld Metal Hydrogen Content

The samples were extracted from the molten weld metal using Vycor tubes at four fixed locations along the length of the weld. These locations were approximately 100, 250, 410, and 560 mm (4, 10, 16 and 22 in.) above the bottom of the weld.

The molten metal samples were quickly quenched in water and kept in dry ice. Each sample was broken into two pieces when cold. The measurements of diffusible hydrogen for each piece were conducted at room temperature using the mercury displacement method of the International Standards Organization (ISO).

Weld Metal Characteristics and Metallography

Once welding was completed, the welds were stored at room temperature for at least two days and then oxygen cut 25 mm (1 in.) away from the weld metal. Four specimens, each with a total weld metal area of 15,800 mm^2 (24.5 $in.^2$) cut from each weld, were metallographically examined.

Two of the specimens were from the bottom (first shoe area), and the remaining two were from the top of the weld (fourth shoe area). The top and bottom specimens were composed of one trans-

$$*B.I.=\frac{CaO+MgO+CaF_2+0.5\ (MnO+FeO)}{SiO_2+0.5\ (Al_2O_3+TiO_2+ZrO_2)}=3$$

Table 1—Hydrogen Values

Weld no.	Electrode[a]	Relative humidity, %	Humidity level	Hydrogen content, $cm^3/100g$ First shoe h_1	Second shoe h_2	Third shoe h_3	Fourth shoe h_4	Average values H_1[b]	H_2[c]
1	L40B	22	Low	4.1	1.9	2.0	1.6	2.0	1.8
2	L40	36	Low	2.8	3.1	2.2	3.0	2.8	2.8
3	L44	24	Low	3.2	2.8	1.8	2.8	2.8	2.5
4	L100	30	Low	4.4	1.5	3.5	2.5	3.0	2.5
5	AW19	16	Low	9.8	3.0	3.9	2.5	3.8	3.2
6	L100	14	Low	3.5	—	1.5	2.0	2.5	1.7
7	L36	15	Low	3.9	2.9	3.2	1.9	3.0	2.7
8	L36	22	Low	2.2	2.3	2.6	2.6	2.5	2.5
9	L40[d]	23	Low	3.0	2.0	3.0	3.3	2.9	2.8
10	AW19	31	Low	4.7	3.1	2.6	2.1	3.0	2.6
11	L36	14	High	11.7	3.2	3.5	2.3	4.7	3.0
12	L40B	26	High	3.8	2.9	3.6	3.5	3.4	3.3
13	L40	13	High	2.0	2.5	3.3	4.3	3.0	3.4
14	L44	13	High	4.2	2.7	2.3	3.2	3.1	2.7
15	AW19	16	High	4.6	2.5	4.4	4.8	4.1	3.9
16	L100	26	High	10.9	3.7	3.2	3.5	5.1	3.5
17	L40[d]	27	High	5.4	4.9	3.4	4.8	4.6	4.4
19	L40	26	High	2.6	2.7	3.1	3.5	3.0	3.1

[a]L—Linde; A—Armco.
[b]$H_1 = \frac{1}{4}(h_1 + h_2 + h_3 + h_4)$
[c]$H_2 = \frac{1}{3}(h_2 + h_3 + h_4)$
[d]2.4 mm (3/32 in.) diameter—all others 3.2 mm (1/8 in.) diameter.

verse and one longitudinal section. The sections were ground and macro-etched. The form factor, which is the ratio of width to depth of the molten pool, was determined from the longitudinal section of the weld metal.

Cracks in the weld metal were detected by using a fluorescent, high sensitivity dye penetrant. The regions containing the cracks were observed at higher magnification. The microstructures, location of cracks and number of cracks were obtained using a Reichert optical microscope. The lengths of the cracks were measured in an IMANCO MR Quantimet 720 microscope assembly. Using the sensitive dye penetrant check and the Quantimet, the shortest crack that could be detected and measured was 0.5mm (0.02 in.) long.

Microhardness (HV_{50}) measurements were conducted on proeutectoid ferrite grains along the prior austenite grain boundaries using a Leitz microhardness tester.

Results

Weld Metal Hydrogen Content

The hydrogen content values of the weld metal are presented in Table 1. The values h_1, h_2, h_3, and h_4 are the average of at least two samples obtained respectively at the top of the first, second, third and fourth shoe level.

Weld Metal Compositions

The chemical composition of all the weld metals is presented in Table 2. Analyses were conducted for other elements, such as O, P, Al, Nb, Zr and V; their percentages (less than 0.02%) were not considered to be significant.

Weld Metal Microstructure

Typical weld metal microstructures that were obtained are shown in Figs. 1 to 4. The microstructures could be classified into three groups—coarse, interme-

Table 2—Weld Metal Chemical Composition, Wt-%

Weld metal	Electrode[a]	C	Mn	Si	S	Cr	Ni	Mo	Cu	Ti
1	L40B	.15	1.15	.09	.016	.010	.03	.23	.07	.014
2	L40	.18	1.54	.09	.019	.01	.03	.18	.07	.016
3	L44	.16	1.45	.01	.013	.04	.28	.22	.16	.01
4	L100	.18	1.60	.10	.017	.20	1.29	.23	.20	.017
5	AW19	.16	.97	.16	.011	.01	1.55	.01	.10	.025
6	L100	.18	1.42	.11	.012	.11	1.22	.24	.12	.013
7	L36	.18	1.29	.02	.013	.04	.02	.01	.08	.01
9	L40[b]	.16	1.31	.01	.010	.03	.01	.22	.07	.01
11	L36	.16	1.35	.01	.013	.03	.02	.01	.06	.01
12	L40B	.16	1.03	.07	.014	.03	.04	.29	.06	.014
13	L40	.18	1.35	.05	.014	.03	.05	.30	.05	.008
14	L44	.16	1.33	.01	.009	.05	.27	.21	.15	.01
15	AW19	.17	.85	.10	.009	.05	1.64	.03	.08	.011
16	L100	.19	1.35	.08	.009	.14	1.21	.26	.14	.008
17	L40[b]	.17	1.17	.04	.010	.02	.03	.31	.05	.003
19	L40	.13	1.38	.04	.014	.21	.23	.28	.17	.008
21	Lo50	.17	1.02	.25	.021	.07	.04	.01	.013	.012

[a]L—Linde; A—Armco; Lo—Lincoln.
[b]2.4 mm (3/32 in. diameter—all others 3.2 mm (1/8 in.) diameters.

Fig. 1—Microstructure and grain boundary crack in the weld metal from electrode L36. 2% nital etch; X100 (reduced 28% on reproduction)

Fig. 2—Microstructure and grain boundary crack in the weld metal from electrode L40B. 2% nital etch; X100 (reduced 28% on reproduction)

Fig. 3—Microstructure and grain boundary crack in the weld metal from electrode AW19. 2% nital etch; X100 (reduced 28% on reproduction)

diate and fine structures.

The coarse grain structures as shown in Figs. 1 and 3 were obtained when the no. L36, AW19 and Lo50 electrodes were used. The structures were characterized by large proeutectoid ferrite grains along the prior austenite grain boundaries. Large proeutectoid grains together with fine two-phase structure (fine pearlite or coarse bainite) were also found inside the prior austenite grains.

An intermediate structure was obtained with 3.2 mm (⅛ in.) L40B and the 2.4 (3/32 in.) L40 electrodes. It was characterized by large proeutectoid ferrite grains mostly along the prior austenite grain boundaries—Fig. 2.

A fine-grain structure was obtained with 3.2 mm (⅛ in.) no. L100, L40, L44 electrodes. This was composed of small proeutectoid ferrite grains along the prior austenite grain boundaries and a very fine structure (proeutectoid ferrite and duplex aggregates or upper bainite) inside the prior austenite grains—Fig. 4. Elements responsible for refining the microstructure were Cr, Mo and Mn and were found in higher levels in these last 3 electrodes.

Weld Metal Cracking

All weld metal cracks were internal and confined to that region of the weld metal where initially the weld gap was present. The number of cracks observed in the weld metal at the bottom (N_B) and the top (N_T) is given in Table 3. The total and average lengths of the cracks at the top (L_T and L_{AT}) and the bottom (L_B and L_{BT}) parts of the weld are also given in Table 3.

Proeutectoid Ferrite Hardness

Microhardness values of the proeutectoid ferrite (average of five values) present at the prior austenite grain boundary are presented in Table 4.

Form Factor

Variations in the form factors were observed from the bottom to the top of the electroslag welds. The average minimum and maximum values were 3.0 and 4.8, respectively.

Discussion

Form Factor and Cracking

In the present study, a minimum value of 3 was observed as the form factor; this, according to Paton (Ref. 26), excludes the possibility of solidification cracks. Solidification cracks followed the dendrit-

Table 3—Weld Metal Crack Measurements[c]

Electrode[a]	Weld no.	N_T	L_T	L_{AT}	N_B	L_B	L_{AB}
L40B	01	0	0	0	2	4.6	2.3
L40	02	0	0	0	1	8.1	8.7
L44	03	0	0	0	4	13.4	3.3
L100	04	0	0	0	2	7.1	3.6
AW19	05	5	19.4	3.9	10	26.5	2.7
L100	06	0	0	0	3	19.9	6.6
L36	07	0	0	0	4	11.1	2.8
L36	08	1	5.3	5.3	2	3.2	1.6
L40[b]	09	2	8.7	4.3	2	5.5	2.8
AW19	10	2	3.3	1.6	18	52.4	2.9
L36	11	0	0	0	6	12.6	2.1
L40B	12	8	28.3	3.5	6	32.9	5.5
L40	13	8	53.5	6.7	0	0	0
L44	14	1	15.7	15.7	2	14.9	7.5
AW19	15	37	123.6	3.3	22	62.0	2.8
L100	16	0	0	0	20	23.3	6.2
L40[b]	17	0	0	0	11	56.4	5.1
Lo50	21	0	0	0	0	0	0

[a] L—Linde; A—Armco; Lo—Lincoln.
[b] 2.4 mm (3/32 in.) diameter—all others 3.2 mm (⅛ in.) diameter.
[c] N_T—number of cracks at top; N_B—number of cracks at bottom; L_T, L_{AT}—total and average length of cracks at top; L_B, L_{AB}—total and average length of cracks at bottom.

Fig. 4—Microstructure and grain boundary crack in the weld metal from electrode L100. 2% nital etch; X100 (reduced 28% on reproduction)

Table 4—Proeutectoid Ferrite Microhardness

Electrode[a]	HV_{50}
L36	207
L40B	205
L40	253
L44	317
L100	321
AW19	216
L40[b]	195

[a]L – Linde; A – Armco
[b]2.4 mm (3/32 in.) diameter – all others 3.2 mm (1/8 in.) diameter

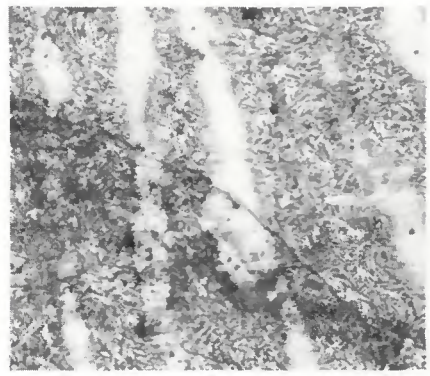

Fig. 5 – Crack in weld metal from electrode L44. Oberhoffer and nital etch, X200 (reduced 28% on reproduction)

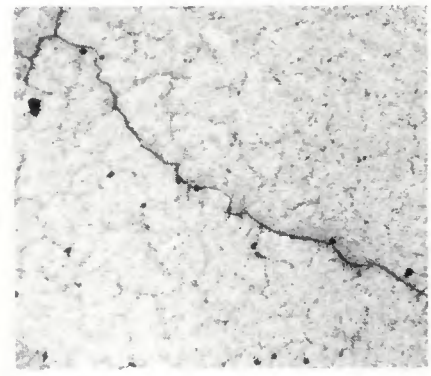

Fig 6 – Electrode L100 weld metal solidification crack with non-solidification propagation part. Oberhoffer and nital etch; X15 (reduced 28% on reproduction)

ic pattern and were, therefore, revealed by etching with the Oberhoffer etchant – Fig. 5. It was confirmed that the grain boundary cracks were not solidification cracks, since they had not propagated through dendrites. Also, grain boundary cracks propagating locally across blocky ferrite grains and ferrite side plates showed that the propagation occurred after the formation of the proeutectoid ferrite.

Few cracks (10%) were identified as solidification cracks and were not included in the crack length measurements. Also, no attempt was made to analyze the incidence of solidification cracks. Figure 6 is a rare example of a crack which had initiated during solidification (on the left side) and propagated straight through the dendrites afterwards.

Hydrogen in the Weld Metal

The hydrogen content along the weld length was not constant. It generally showed a higher concentration of hydrogen (see Table 1) at the bottom. Similar observations have been reported in the literature (Ref. 25-27). Measurements at the upper three locations of the weld showed that the hydrogen content had reached an equilibrium, since it remained almost constant. In fact, there was a small accumulation of hydrogen along the length of the welds as already noted by Paton (Ref. 26). There was also an average increase of 1.3 cm^3/100 g of diffusible hydrogen, for every meter of weld length, observed under high humidity conditions. The high humidity condition was equivalent to 80% relative humidity (R.H.) at 30°C (86°F) and was comparable to that of a hot humid day (Ref. 18). The low humidity level was comparable to that of a normal day.

The variation of hydrogen content in the weld metal for identical conditions of welding was probably due to the difficulty in maintaining the air humidity constant above the slag (variation in ambient R.H.). The present study showed that an average hydrogen content of 2.5 cm^3/100 g yielded cracks at the top portions of the welds performed with the no. L36 (one crack, 5.3 mm or 0.21 in. long) or AW19 (5 cracks, 3.9 mm or 0.15 in. average length) electrodes.

The total number of cracks obtained from the welds increased (i.e., multiplied) by a factor of 3.5 due to the 40%, increase in diffusible hydrogen content when the higher humidity conditions were used. This corresponded to an average total increase in hydrogen content obtained from all the welds by a factor of 1.4, i.e., from 2.8 to 3.9 cm^3/100 g. Also, there was a 40% increase in the average crack length. This, once again, verified the observation that the humidity content of the atmosphere above the fused slag played a major role in the formation of the hydrogen cracks observed in the electroslag welds.

Separate Treatments of the Results Obtained from the Bottom and Top Portions of the Weld

The crack measurements (number and lengths) were kept separated between top and bottom portions of the welds for the following reasons:

1. The hydrogen measurements showed larger variations at the bottom of the weld.
2. As the weld progressed, the restraint was expected to vary and be more stable at the top.
3. The heating and cooling cycles varied from bottom to top, due to a preheat effect as welding progressed.

The reproducibility of the results for the top portion was therefore expected to be better.

Multilinear Regression Analysis (MLRA)

A comparison of the hydrogen levels and the cracking in the welds, performed at two humidity levels for various elec-

Table 5—MLR Coefficients Including Titanium

	Crack status[a]		
	N_T	L_T	L_{AT}
Cr	−24.7	−151.2	−28.7
Cu	−33.6	−97.5	46.8
H	3.2	16.0	.83
Mn	−32.0	−85.7	1.5
Mo	9.8	49.1	−0.2
Ni	20.6	61.3	−7.6
Si	−135.4	−328.4	58.5
S	2691	7334	−1410
Ti	−944	−3654	11.6
Y_i[b]	$Y_1 = 15.0$	$Y_2 = 33.5$	$Y_3 = 13.0$
M.C.C.[b]	0.91	0.90	0.71
SEE[b]	5.1	20.0	3.9

[a]N_T – number of cracks at top; L_T, L_{AT} – total and average length of cracks at top.
[b]Y_i – intercept; M.C.C. – multiple correlation coefficient; SEE – standard error of estimate.

Table 6—MLR Coefficients Including Carbon

	Crack status[a]		
	N_T	L_T	L_{AT}
C	111.3	426	51.1
Cr	32.0	67.9	−29.3
Cu	−67.2	−230.7	61.2
H	3.6	17.7	0.7
Mn	−39.4	−11301	−2.6
Mo	16.1	73.4	0.6
Ni	15.2	40.3	−8.1
Si	−164.2	−439	54.7
S	2248	5597	−1309
Y_i[b]	$Y_1 = 1.86$	$Y_2 = -16.2$	$Y_3 = 7.8$
M.C.C.[b]	0.91	0.85	0.72
SEE[b]	6.01	23.6	3.8

[a]N_T – number of cracks at top; L_T, L_{AT} – total and average length of cracks at top.
[b]Y_i – intercept; M.C.C. – multiple correlation coefficient; SEE – standard error of estimate.

trodes, showed that cracking could not be analyzed by considering the hydrogen levels alone. The weld metal composition, which would play a major role in hydrogen cracking, was also considered; and a MLRA was carried out to relate weld metal composition to hydrogen cracking.

Most chemical composition variations were considered to be rather small—Table 2. Hence, it was considered that the number of cracks and their total or average length could be linearly related to chemical composition (including diffusible hydrogen) as follows:

$$N_T = y_1 + a_1C + b_1Mn + c_1 Si + d_1Cr + e_1Ni + f_1Mo + g_1S + h_1 Cu + i_1Ti + j_1H_2$$

$$L_T = y_2 + a_2C + b_2Mn + c_2 Si + d_2Cr + e_2Ni + f_2Mo + g_2S + h_2Cu + i_2Ti + j_2H_2$$

$$L_{AT} = y_3 + a_3C + b_3Mn + c_3 Si + d_3Cr + e_3Ni + f_3Mo + g_3S + h_3 Cu + i_3Ti + j_3H_2$$

Where L_T and L_{AT} are in mm, chemical compositions C, Mn, etc. . . are in wt-%, H_2 is in $cm^3/100$ g, a_i to j_i are coefficients of the MLRA and y_i is the intercept (i = 1 to 3). The problem was then to solve 3 systems of 19 equations (19 welds) with 10 independent variables. Weld nos. 8 and 10 were the repeats of weld nos. 7 and 5 respectively; for this reason, their chemical compositions were considered to be respectively identical.

Because the matrix (Tables 2 and 3) was redundant (too many variables), two types of computation had to be made with 9 variables instead of 10; the two variables permutated were C and Ti. Computations were performed on bottom and top data. Results showed that the multiple correlation coefficient (MCC), and the standard error of estimate (SEE) were consistently lower for the bottom portion of the weld. The results, therefore, confirmed the previous assumption that there would be a better reproducibility of the results for the top portion of the welds. The MLR coefficients a_i-j_i and the intercept y_i obtained for the top portion of the welds are presented in Tables 5 and 6.

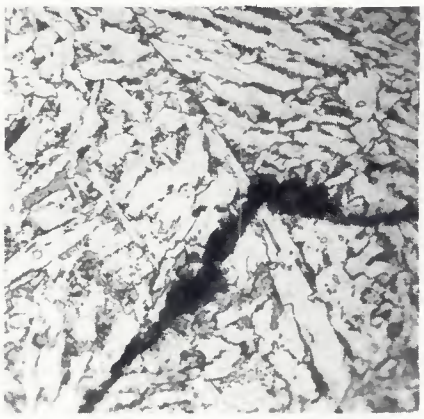

Fig 7—Electrode L100 weld metal microstructure and crack. 2% nital etch; X1000 (reduced 28% on reproduction)

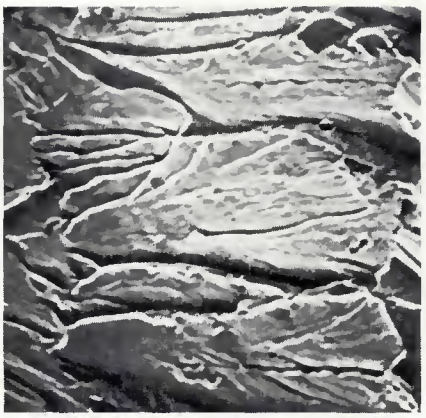

Fig. 8—SEM fractograph of intergranular crack in weld metal from 2.4 mm (3/32 in.) diameter electrode L40 (weld no. 17). X1300 (reduced 32% on reproduction)

The average values of the MLR coefficients calculated from Tables 5 and 6 are presented in Table 7. It is to be noted that a negative coefficient was related to a beneficial effect while a positive coefficient was related to a detrimental effect (with respect to cracking). The MLR coefficients of Si, Cu, H, Ni and S have the same signs in Tables 5 and 6, but the MLR coefficients of Cr, Mn and Mo in Tables 5 and 6 do not yield the same sign. The elements in Table 7 could be divided into five groups based on their effects on nucleation (N_T), propagation (L_{AT}), and the total length (L_T) of the cracks:

Group 1: H, Mo and C. These were detrimental elements which aided the nucleation, propagation and total length of the cracks, even though Mo did not seem to have a strong effect on the propagation of the cracks.

Group 2: Ni and S. These elements had an intermediate effect on cracking. They enhanced nucleation and increased the total length of the cracks but lowered the average crack length, thus reducing the propagation of cracks. In this case, the beneficial effect of reduction in propagation was compensated by the detrimental effect of increase in nucleation.

Group 3: Si, Ti, Cu. Contrary to Group 2, these elements had a beneficial influence on nucleation by reducing the number of cracks. Even though they contributed to the propagation of cracks by increasing their average length, they decreased the total crack length. Again, the beneficial effect of nucleation was balanced by the propagation of the crack.

Group 4: Cr. Referring to Tables 5 and 6, Cr showed mixed effects on nucleation and the total length of cracks and, therefore, was considered carefully. In any case, Cr appeared to be effective in reducing the propagation ability of the cracks while mildly enhancing nucleation.

Group 5: Mn. There was strong evidence that Mn was beneficial in reducing all three factors—N_T, L_T, and L_{AT}.

The reversible-irreversible hydrogen trap problem (diffusible occluded hydrogen) was met here with sulfur (MnS inclusions) and Ti. Sulfur, in the form of inclusions, would have a strong trapping effect on hydrogen, but these traps would also act as crack nuclei. On the one hand, inclusions would act beneficially by trapping hydrogen and would reduce the diffusible hydrogen available for crack propagation; on the other hand, larger inclusions would also act as local stress raisers. This would explain the larger number of crack nuclei created together with a smaller average crack length in this work.

With respect to Ti, TiC is known to exert a strong attraction on diffusible hydrogen and distribute it uniformly (Ref. 27); this would be beneficial. Unfortunately, the total amount of hydrogen stored by the weld metal would be increased giving a longer average crack.

Table 7—Combined Average M.L.R. Coefficients Related to Number of Cracks (N_T), Total Length of Cracks (L_T), and Average Length of Cracks (L_{AT})—Obtained from Tables 5 and 6

	N_T	L_T	L_{AT}
C	113.3	426.0	51.1
Cr	3.7	−41.7	−29.0
Cu	−50.4	−164.1	54.0
H	3.3	16.8	0.76
Mn	−35.7	−99.4	−0.55
Mo	13.0	61.3	0.20
Ni	17.9	50.7	−7.9
Si	−149.8	−383.7	56.6
S	2470	6466	−1360
Ti	−944	−3654	11.6
Y_i[a]	Y_1 = 8.4	Y_2 = 8.7	Y_3 = 10.4

[a] Y_i = intercept.

Fractographic Examination of the Crack Surface

It was observed that electrodes such as L100, L40 and L44 eliminated the blocky

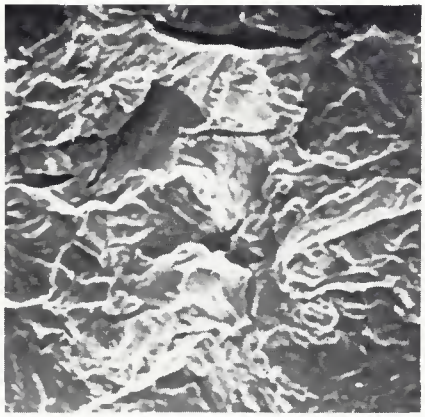

Fig. 9—SEM fractograph of intergranular crack in electrode L40 weld metal. X1200 (reduced 32% on reproduction)

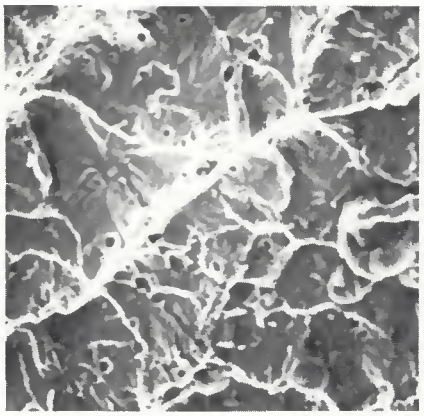

Fig. 10—SEM fractograph of intergranular crack in electrode AW19 weld metal (weld no. 15). X1000 (reduced 32% on reproduction)

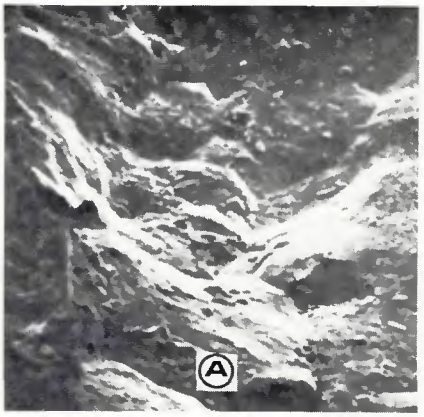

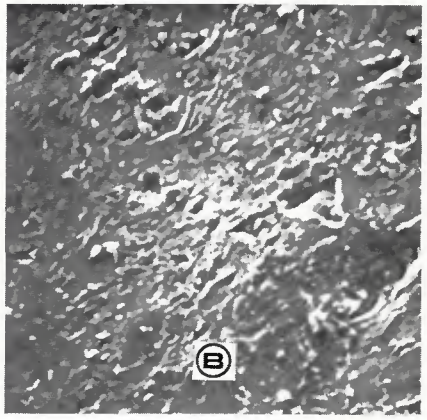

Fig. 11—SEM fractograph of the intergranular crack in electrode L100 weld metal. A—X450; B—X950 (reduced 32% on reproduction)

proeutectoid ferrite veins in the weld metal. In fact, in weld metal deposited using no. L100 electrode, the prior austenite grain boundary was still constituted of proeutectoid ferrite (but rather refined, acicular instead of blocky shaped) and the cracks were still located along the grain boundaries—Fig. 7.

The typical fractographic appearances of weld metal cracks shown in Figs. 8–10 are characterized by large blocky ferrite grains along the prior austenite grain boundaries. The features on these ferrite grains could be described as quasi-cleavage. There was a noticeable difference in fractographic appearance of the cracks in the electroslag welds performed with L100 electrodes—Fig. 11A. In this case the intergranular aspect (with respect to the prior austenite grains) appeared more prominently, while quasi-cleavage could not be seen—Fig. 11B.

The above variation in the microscopic propagation mode of the cracks was probably due to the size of the ferrite grains. Therefore, the weld crack propagation mode was intergranular (with respect to the prior austenite grain boundary) when the stress intensity factor K_1 was low. The fractographic aspects, nonetheless, depended on the degree of refinement of the proeutectoid ferrite grains or on the amount of Mo, Mn, Cr and Ni present in the weld metal.

It should be noted that increasing the hardenability of the weld metal with Mn, Mo, Cr and Ni would have two competing effects on crack nulceation N_T. Although the ferrite veins would be strengthened (grain refinement), the amount of diffusible hydrogen would most likely be increased (Ar_3 would decrease and the carbide-matrix interface area would increase).

Most microstructure refiners (Cr, Ni, Mn) were on the beneficial side when considering the average crack length, L_{AT}. Mo was an exception; this apparently had a negligible effect on L_{AT}. From this, it was concluded that the overall effect of these elements was beneficial. The present results on the average crack length (Table 7) indicated that Cr and Ni contents could be increased to improve the resistance to cracking; on the other hand, Mo and Mn contents should not exceed the maximum values used in the present work.

Many inclusions were seen at the surface of the cracks in electroslag welds made with the L100 electrode. In addition, both microvoids and inclusions were observed in the cracks found in the electroslag welds performed with the AW19 electrode (high hydrogen contents).

Ferrite Microhardness and Average Crack Length

Linear regression analysis of the microhardness of the ferrite and the average crack length for the top portion of the welds showed that an increase of 50 HV_{50} in hardness was accompanied by an increase of 2 mm (0.08 in.) in the average crack length (the correlation coefficient is 0.85). The present work showed that Si was the main element responsible for enhancing the crack propagation (L_{AT}; refer to Table 7), and could be related to the ferrite hardening property of Si.

Conclusions—A Summary of Results

1. Hydrogen cracks were found in electroslag weld metals propagating along the prior austenite grain boundaries even with electrodes which produce refined microstructures (L100) in the weld metal.

2. Two humidity levels (comparable to that of a normal day and of a hot humid day) resulted in average total hydrogen content in the weld metal of 2.8 $cm^3/100$ g and 3.9 $cm^3/100$ g respectively. Also the hydrogen content at the bottom of the weld was generally much higher than along the length of the rest of the weld.

3. While hydrogen content increased 40% as a result of change in humidity levels, the average number of cracks was increased approximately by a factor of 3.5 and the average crack length was increased by a factor of 1.4 (from 3.9 to 5.5 mm or 0.15 to 0.22 in.). All cracks were internal and confined to that region of the weld metal where initially the weld gap was present.

4. There was a marked change in the microstructure. L100, L44 and L40 electrodes produced a refined structure with almost no ferrite veins, whereas L36 and L40B, as well as Lo50 and AW19 electrodes, produced blocky ferrite grains along the prior austenite grain boundary. The refined structure was due to the presence of higher Cr, Mo, Mn, C or Ni content in the nos. L100, L44 and L40 electrodes.

5. As expected, carbon and hydrogen enhanced both the nucleation and propagation stages of cracking.

6. The results are consistent with the theories stating that sulfur in the form of manganese sulfide inclusions, although acting as crack nuclei, could also trap hydrogen and decrease the average crack length.

7. Chromium and nickel up to a maximum of 0.5 and 2%, respectively, could be recommended to reduce the average

length of hydrogen cracks, however they would increase the number of cracks.

8. Silicon, titanium and copper were clearly detrimental as far as the length of crack was concerned. They should be kept at low levels ($Si < 0.1\%$, $Cu < 0.1\%$). Although titanium increased the crack length, it decreased drastically the number of cracks.

9. Molybdenum and manganese had mild detrimental and beneficial effects on the crack propagation, respectively, and should be considered in order to achieve mechanical property requirements only after maximum levels of Cr and Ni had been reached.

Acknowledgment

The authors wish to thank their colleagues within the AMCA International Research and Development Laboratory whose help has been greatly appreciated. The research program was partially funded by the National Research Council of Canada and undertaken in the Corporate AMCA International R&D Centre which gave permission for the publication of this paper.

References

1. Graville, B. A. 1975. *The principles of cold cracking control in welds.* Dominion Bridge Company Limited.

2. Million, A., and Million, C. 1971. *L'hydrogene dans les aciers et dans les joints soudes.* Paris: Dunod.

3. Smialowski, M. 1962. *Hydrogen in steel.* Pergamon Press.

4. Koslov, R. A., and Kiselev, Ya. N. 1977. The effects of alloying elements on the hydrogen embrittlement of medium alloy deposited metal. *Welding Production* 24:30-33.

5. Bastien, P. 1972. L'action de l'hydrogene sur le fer et les aciers et ses consequences dans l'industrie. Congress international: *L'hydrogene dans les metaux.* pp. 11-30. Edited Sciences et Industries. Paris.

6. Hirth, J. P. 1980. Effects of hydrogen on the properties of iron and steel. *Met. Trans.* 11A:861-890.

7. Bernstein, I. M., and Thomson, A. W. 1979. Effect of structural inhomogeneities on the hydrogen embrittlement of steel. *Proceedings JIM IS-2, hydrogen in metals,* pp. 429-432.

8. Rollason, E. C. and Roberts, R. R. 1950 (Oct.). Effect of cooling rate and composition on the embrittlement of weld metal. *Jour. of The Iron and Steel Inst.,* pp. 105-112.

9. Oriani, R. A. 1972. A mechanistic theory of hydrogen embrittlement of steels. *Ber. Der Bunsen, Coescelsch of Phys. Chem,* 76:301-310.

10. Petch, N. J. 1956. Lowering of the fracture stress due to adsorption. *Phil. Mag.* 1:331-337.

11. Tetelman, A. S. 1963. *The hydrogen embrittlement of ferrous alloys,* pp. 671-707. New York: Interscience.

12. Zapffe, C. C., and Sims, C. E. 1941. Hydrogen embrittlement, internal stress and defects in steel. *Trans. AIME* 145:225-261.

13. Beachem, C. C. 1972. A new model for hydrogen assisted cracking. *Met. Trans.* 3:259-273.

14. Bernstein, I. M. 1970. The role of hydrogen in the embrittlement of iron and steel. *Mat. Sci. Eng.* 6:1-19.

15. Tyson, W. 1979. Hydrogen in metals. *Can. Met. Quart.* 18:1-11.

16. Oriani, R. A. 1978. Hydrogen embrittlement of steels. *Ann. Rev. Mat. Sc.* 8:327-357.

17. Cornet, M., and Talbot-Besnard. 1972. Fragilisation du fer de haute purete par l'hydrogene, influences de faibles additions de carbone. Congress international: *L'hydrogene dans les metaux.* Ed. Sciences et Industries. Paris.

18. Konkol, P. J., and Domis, W. F. 1979. Causes of grain boundary separations in electroslag weld metals. *Welding Journal* 58(6):161-s to 165-s.

19. Boniszewski, T., and Watkinson, F. 1973. Effect of weld microstructures on hydrogen induced cracking in transformable steels: part I and part II. *Metals and materials,* pp. 90-96 and 145-151.

20. Mabuchi, H., and McMahon, C. J. 1979. Further observations of compositional and aging effects on hydrogen induced cracking of HY130 steels. *Proc. JIMIS-2 hydrogen in metals,* pp. 441-444.

21. Kameda, J., Bondyopadhyay, N., and McMahon, C. J., Jr. 1979. Hydrogen-induced fracture in alloy steels. *Proc. of JIMIS-2 hydrogen in metals,* pp. 437-440.

22. Yoshigawa, S., and Shumuchi Tonezawa. 1979. Crack growth rate of high strength steel as a function of hydrogen content. *Proc. JIMIS-2 hydrogen in metals,* pp. 445-448.

23. Matsuda, F., Nakagawa, H., Tsuji, T., and Tsukomoto, M. 1978. Fractography of cold crack of various carbon steels and alloy steels by means of the implant test. *Trans. JWRI* 7:71-85.

24. Hart, P. H. 1980 (Nov.). *Hydrogen cracking in weld metals—the effect of manganese.* Welding Institute res. bull., pp. 327-333.

25. Lowe, G., Bala, S. R., and Malik, L. 1981. Hydrogen in consumable guide electroslag welds—its sources and significance. *Welding Journal* 60(12):258-s to 268-s.

26. Paton, B.E. 1962. *Electroslag welding.* 2nd ed. American Welding Society.

27. Mitchell, A., and Smailer, R. M. 1979. Practical aspects of electroslag remelting technology. *International Metal Rev.* 24:231-264.